Journal of Japan Association for Earthquake Engineering, Vol. 22, No. 3, 2022

DETECTION OF STEP AND PULSE COMPONENTS AND ESTIMATION OF DISPLACEMENT WAVEFORM BASED ON NEAR-FAULT SEISMIC GROUND MOTION RECORD

Takashi HIRAI[1]

[1] Member, Dr. Eng., Assistant Professor, Disaster Mitigation Research Center, Nagoya University, Nagoya, Japan, hirai.takashi@nagoya-u.jp

ABSTRACT: In this study, a method for detecting the step and pulse components as well as estimating the displacement waveform based on seismic ground motion records was developed. These components represent the residual displacement and pulse-like ground motion in the near-fault region. In addition, the displacement waveforms were synthesized by combining the observed Fourier spectrum and obtained model spectrum instead of using a low-cut filter. Applying the proposed method to strong ground motion records during the mainshock of the 2016 Kumamoto earthquake, the displacement waveforms containing the step and pulse components were appropriately estimated.

Keywords: *Near-fault seismic ground motion, Displacement waveform, Spectral fitting, Kumamoto earthquake*

1. INTRODUCTION

Displacements due to earthquakes contain useful information for analyzing seismic source processes and dynamic characteristics of soil, estimating damages to structures, and so on. Particularly, significant ground motions, including large residual displacements and impulsive motions, occur near seismic faults, causing serious damages to structures at times. Ground motion records containing such significant motions are often observed recently due to an increase in density of strong motion-observation sites (e.g., Iwata[1)]).

Usually, strong ground motion records are obtained as acceleration waveforms, although acceleration and velocity seismometers are used. Residual and impulsive displacements are obtained as a double integral of the acceleration record because servo accelerometers have flat frequency characteristics, including direct current (DC) components. However, displacement waveforms cannot be accurately obtained in many cases due to low-frequency noise and baseline change caused by a tilt of the sensor (e.g., Graizer[2)]).

To estimate displacement waveforms from actual acceleration records, the effect of noise components and baseline change should be eliminated. A change in the acceleration baseline appears as a straight trend in velocity waveforms obtained by integrating acceleration records. Boore[3)], Ohta and Aydan[4)], and Hirai and Fukuwa[5)] estimated the occurrence time and the amount of change in the acceleration baseline by fitting the trend of a velocity waveform to a linear function. Iwan et al.[6)]

proposed a method to correct the acceleration baseline by approximating the velocity waveform as a set of linear functions defined in three sections. These methods are applied in the time domain, whereas Javelaud et al.[7] and Motoyama and Murono[8] proposed methods to correct the acceleration baseline in the frequency domain. In general, once the effect of the acceleration baseline change is removed, a reasonable displacement waveform is obtained by integrating the acceleration record.

However, even if the abovementioned methods are applied, a reasonable displacement waveform may not be obtained due to the residual effect of the baseline change or other noise components. Although the low-frequency noise can be removed by the low-cut filter via the Fourier transform, it becomes difficult to obtain the residual and impulsive displacements in this case because most of the power of these components is in the low-frequency range. To use the low-cut filter means that the value of the Fourier spectrum is assumed to be zero under the cut-off frequency, though residual and impulsive components have finite values in that region. To resolve the inconsistency, Hayashi et al.[9] proposed to reduce the distortion of displacement waveform integrating only the real part of the acceleration Fourier spectrum because the contribution of the real part of the Fourier spectrum is greater than that of the imaginary part. In addition, Hirai[10] proposed to assign the low-frequency component of the displacement Fourier spectrum connecting the trapezoidal function component that simulates the overall shape of displacement waveforms with the residual component by spectral fitting. However, the method is available when the residual component is dominant in a displacement waveform, whereas it is not applicable for an impulsive displacement waveform.

In this study, two basic functions are defined to model the step and pulse components of a displacement waveform near the seismic fault, which correspond to the residual and impulsive components of displacement, respectively. These functions are detected from the strong ground motion records by spectral fitting and then used to estimate displacement waveforms by connecting their Fourier spectra in the low-frequency region instead of using the low-cut filter. In addition, the proposed method is applied to the strong ground motion records of the 2016 Kumamoto earthquake. The spatial distribution of the residual displacement is compared with that by Global Navigation Satellite System (GNSS) observation. This paper is based on the presentation at the 2019 Annual Meeting of the Japan Association for Earthquake Engineering by the author[11].

2. FORMULATION

2.1 Basis functions modeling displacement waveform

In this study, two features of the near-fault displacement waveform are represented by the step and pulse components, which correspond to the component causing the residual displacement and the displacement that returns to the origin after swaying to the positive or negative direction, respectively. According to the theory of elasticity, a displacement waveform around the seismic source fault comprises two kinds of terms proportional to the time series of the fault slip and its derivative. Assuming that the former and latter correspond to the step and pulse components, respectively, the velocity and acceleration of the step component are, respectively, represented by the first and second derivatives of the basis function. Similarly, the displacement, velocity and acceleration of the pulse component are represented by the first, second and third derivatives of the basis function, respectively. In this study, three types of basis function were examined: Gaussian, sine wave and polynomial types. Figure 1 shows their shapes.

The Gaussian-type basis function represents the step displacement by a cumulative normal distribution function. In this case, the shape of the acceleration of the pulse component is similar to the Ricker wavelet. This basis has been used in other studies for modeling the near-fault ground motion (e.g., Kostadinov and Yamazaki[12]) and the evaluation of the building response to the impulsive ground motion (e.g., Okazawa et al.[13]). The basis function and its first, second and third derivatives are, respectively, defined as follows:

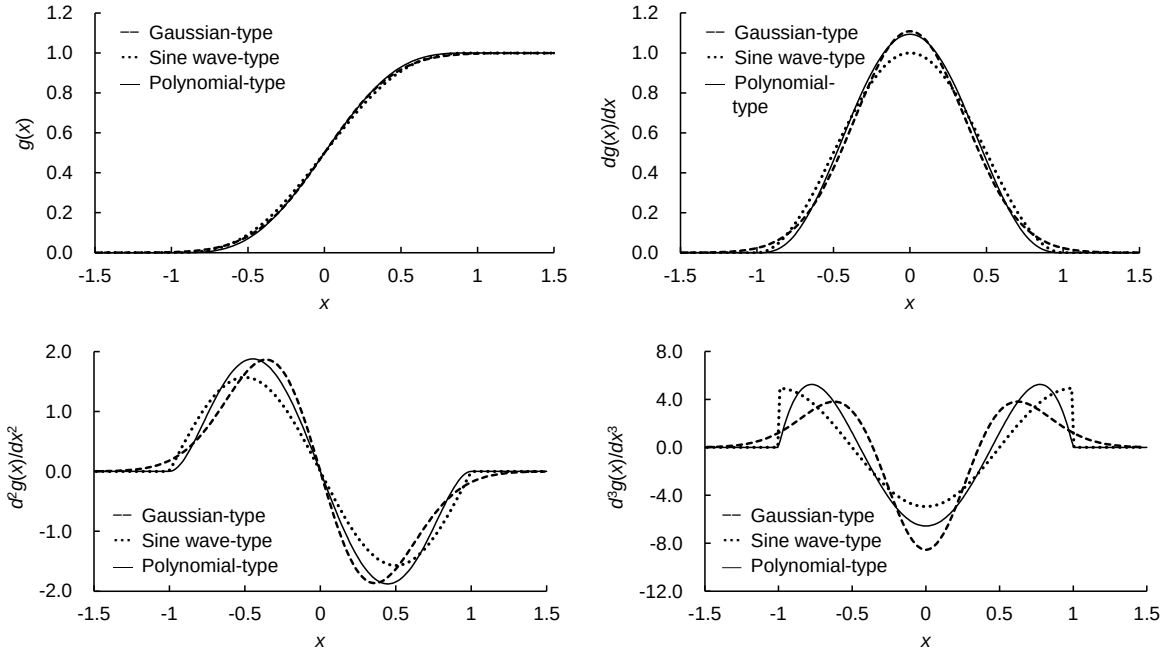

Fig. 1 Graphs of the basis function $g(x)$ and its first, second and third derivatives

$$g(x)=\int_{-\infty}^{x}\frac{1}{\sqrt{2\pi}\sigma}e^{-\frac{\xi^2}{2\sigma^2}}d\xi \tag{1}$$

$$g'(x)=\frac{dg(x)}{dx}=\frac{1}{\sqrt{2\pi}\sigma}e^{-\frac{x^2}{2\sigma^2}} \tag{2}$$

$$g''(x)=\frac{d^2g(x)}{dx^2}=-\frac{x}{\sqrt{2\pi}\sigma^3}e^{-\frac{x^2}{2\sigma^2}} \tag{3}$$

$$g'''(x)=\frac{d^3g(x)}{dx^3}=\frac{1}{\sqrt{2\pi}\sigma^3}\left(\frac{x^2}{\sigma^2}-1\right)e^{-\frac{x^2}{2\sigma^2}}, \tag{4}$$

where the constant σ is determined as 0.36 to give $g'(x)$ the frequency characteristics equivalent to that of the polynomial-type basis function.

The sine wave-type basis function represents the acceleration of the step component by a period of the sine wave. This basis function has also been used for modeling the near-fault ground motion (e.g., Moriwaki[14]) and evaluating the building response to the impulsive ground motion (e.g., Yasumoto et al.[15]). The basis function and its first, second and third derivatives are, respectively, defined as follows:

$$g(x)=\{U(x+1)-U(x-1)\}\left\{\frac{1}{2}(x+1)+\frac{1}{2\pi}\sin\pi x\right\}+U(x-1) \tag{5}$$

$$g'(x)=\frac{1}{2}\{U(x+1)-U(x-1)\}(1+\cos\pi x) \tag{6}$$

$$g''(x)=-\frac{\pi}{2}\{U(x+1)-U(x-1)\}\sin\pi x \tag{7}$$

$$g'''(x)=-\frac{\pi^2}{2}\{U(x+1)-U(x-1)\}\cos\pi x, \tag{8}$$

where $U(x)$ denotes the unit step function. These functions vary in the range $-1 \le x \le 1$ but are constants outside.

Although the Gaussian- and sine wave-type basis functions are widely used in other studies, they have unnatural features as the model function of the seismic ground motion. Since the Gaussian-type basis function never becomes zero strictly, the displacement waveform does not satisfy the causality regardless of the rise time of the residual displacement. Moreover, the acceleration waveform of the pulse component modeled by the sine wave-type basis function is discontinuous at $x = -1$ and $x = 1$. To solve such unnatural features, the polynomial-type basis function is defined to satisfy boundary conditions: the values are zero in the range $x < -1$, and the third derivative is continuous at $x = -1$ and $x = 1$. The basis function and first, second and third derivatives are, respectively, defined as follows:

$$g(x) = \frac{1}{32}\{U(x+1) - U(x-1)\}\left(16 + 35x - 35x^3 + 21x^5 - 5x^7\right) + U(x-1) \tag{9}$$

$$g'(x) = \frac{dg(x)}{dx} = \frac{35}{32}\{U(x+1) - U(x-1)\}\left(1 - 3x^2 + 3x^4 - x^6\right) \tag{10}$$

$$g''(x) = \frac{d^2 g(x)}{dx^2} = \frac{105}{16}\{U(x+1) - U(x-1)\}\left(-x + 2x^3 - x^5\right) \tag{11}$$

$$g'''(x) = \frac{d^3 g(x)}{dx^3} = \frac{105}{16}\{U(x+1) - U(x-1)\}\left(-1 + 6x^2 - 5x^4\right), \tag{12}$$

where the coefficient of each term is determined from the conditions $g(0) = 1/2$, $g(1) = 1$ and $g'(1) = g''(1) = g'''(1) = 0$. These functions vary in the range $-1 \le x \le 1$, and only $g(x)$ produces the residual displacement.

2.2 Representation of ground motion waveform using basis functions

Applying basis functions, the step and pulse components contained in the near-fault GM are represented. Subscripts d, v and a denote displacement, velocity and acceleration, respectively.

$$\phi_{\mathrm{d}}(t) = g\left(\frac{t - t_{\mathrm{d}}}{t_{\mathrm{m}}}\right), \quad \phi_{\mathrm{v}}(t) = \frac{1}{t_{\mathrm{m}}} g'\left(\frac{t - t_{\mathrm{d}}}{t_{\mathrm{m}}}\right), \quad \phi_{\mathrm{a}}(t) = \frac{1}{t_{\mathrm{m}}^2} g''\left(\frac{t - t_{\mathrm{d}}}{t_{\mathrm{m}}}\right) \tag{13}$$

$$\psi_{\mathrm{d}}(t) = Cg'\left(\frac{t - t_{\mathrm{d}}}{t_{\mathrm{m}}}\right), \quad \psi_{\mathrm{v}}(t) = \frac{C}{t_{\mathrm{m}}} g''\left(\frac{t - t_{\mathrm{d}}}{t_{\mathrm{m}}}\right), \quad \psi_{\mathrm{a}}(t) = \frac{C}{t_{\mathrm{m}}^2} g'''\left(\frac{t - t_{\mathrm{d}}}{t_{\mathrm{m}}}\right), \tag{14}$$

where t_{d} and t_{m} denote the center and half-length of the duration of the displacement rising. Each coefficient C in Eq. (14) is the normalization factor to make the residual displacement unity, namely, $\sqrt{2\pi}\sigma$, 1 and 32/35 for the Gaussian-, sine wave- and polynomial-type basis functions, respectively. Fourier spectra of Eqs. (13) and (14) are, respectively, as follows:

$$\Phi_{\mathrm{d}}(\omega) = \frac{1}{i\omega} e^{-i\omega t_{\mathrm{d}}} G'(\omega t_{\mathrm{m}}), \quad \Phi_{\mathrm{v}}(\omega) = e^{-i\omega t_{\mathrm{d}}} G'(\omega t_{\mathrm{m}}), \quad \Phi_{\mathrm{a}}(\omega) = i\omega e^{-i\omega t_{\mathrm{d}}} G'(\omega t_{\mathrm{m}}), \tag{15}$$

$$\Psi_{\mathrm{d}}(\omega) = t_{\mathrm{m}} C e^{-i\omega t_{\mathrm{d}}} G'(\omega t_{\mathrm{m}}), \quad \Psi_{\mathrm{v}}(\omega) = i\omega t_{\mathrm{m}} C e^{-i\omega t_{\mathrm{d}}} G'(\omega t_{\mathrm{m}}), \quad \Psi_{\mathrm{a}}(\omega) = -\omega^2 t_{\mathrm{m}} C e^{-i\omega t_{\mathrm{d}}} G'(\omega t_{\mathrm{m}}), \tag{16}$$

where the representation of $\Phi_{\mathrm{d}}(\omega)$ is available to $\omega \neq 0$. $G'(u)$ is the Fourier transform of $g'(x)$, given for each basis function as follows:

Gaussian type: $$G'(u) = e^{-\frac{\sigma^2 u^2}{2}} \tag{17}$$

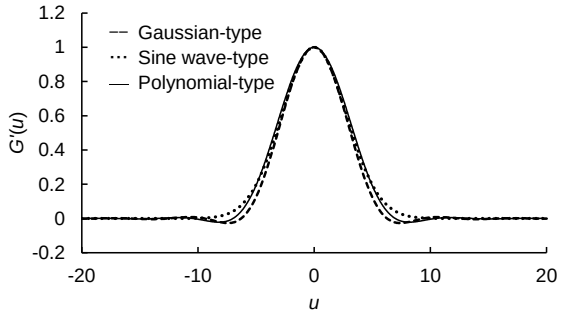

Fig. 2 Fourier spectrum $G'(u)$ of the first derivative of basis function $g'(x)$

Sine wave type: $$G'(u) = \operatorname{sinc} u + \frac{1}{2}\operatorname{sinc}(u-\pi) + \frac{1}{2}\operatorname{sinc}(u+\pi) \tag{18}$$

Polynomial type: $$G'(u) = \begin{cases} 105\left(\frac{1}{u^4} - \frac{15}{u^6}\right)\cos u + 315\left(-\frac{2}{u^5} + \frac{5}{u^7}\right)\sin u & (u \neq 0) \\ 1 & (u = 0) \end{cases}, \tag{19}$$

where sinc means unnormalized cardinal sine function defined as

$$\operatorname{sinc} z = \begin{cases} (\sin z)/z & (z \neq 0) \\ 1 & (z = 0) \end{cases}. \tag{20}$$

Figure 2 shows the real part of $G'(u)$. Since $g'(x)$ is a real-valued even function for each basis function, $G'(u)$ is also a real-valued even function.

2.3 Detection of step and pulse components by spectral fitting

The ground motion near the seismic fault is approximately modeled by the linear combination of step and pulse components.

$$d_{\mathrm{m}}(t) = \alpha\phi_{\mathrm{d}}(t) + \beta\psi_{\mathrm{d}}(t) \tag{21}$$

$$v_{\mathrm{m}}(t) = \alpha\phi_{\mathrm{v}}(t) + \beta\psi_{\mathrm{v}}(t), \tag{22}$$

Hereinafter, d_{m} and v_{m} are called model displacement and velocity, respectively. α and β denote magnitudes of step and pulse components, respectively. Their Fourier spectra are expressed as follows, separating into real and imaginary parts:

$$D_{\mathrm{m}}(\omega) = G'(\omega t_{\mathrm{m}})\left[\left\{C\beta t_{\mathrm{m}}\cos\omega t_{\mathrm{d}} - \alpha t_{\mathrm{d}}\frac{\sin\omega t_{\mathrm{d}}}{\omega t_{\mathrm{d}}}\right\} + \left\{-\alpha t_{\mathrm{d}}\frac{\cos\omega t_{\mathrm{d}}}{\omega t_{\mathrm{d}}} - C\beta t_{\mathrm{m}}\sin\omega t_{\mathrm{d}}\right\} i\right] \tag{23}$$

$$V_{\mathrm{m}}(\omega) = G'(\omega t_{\mathrm{m}})\left[\left\{\alpha\cos\omega t_{\mathrm{d}} + C\beta\omega t_{\mathrm{m}}\sin\omega t_{\mathrm{d}}\right\} + \left\{C\beta\omega t_{\mathrm{m}}\cos\omega t_{\mathrm{d}} - \alpha\sin\omega t_{\mathrm{d}}\right\} i\right], \tag{24}$$

where the representation of $D_{\mathrm{m}}(\omega)$ is available to $\omega \neq 0$. In general, t_{d} is greater than t_{m}, making the shapes of these spectra a carrier wave of angular frequency t_{d} in the envelope $G'(\omega t_{\mathrm{m}})$ in the frequency domain. The behaviors of Eqs. (23) and (24) should be considered carefully because the envelope $G'(\omega t_{\mathrm{m}})$ has a large value in the low-frequency region. The limit values of the real and imaginary parts of each spectrum in the low-frequency region are as follows:

$$\lim_{\omega\to+0}\mathrm{Re}\left[D_{\mathrm{m}}(\omega)\right]=-\alpha t_{\mathrm{d}}+C\beta t_{\mathrm{m}},\quad \lim_{\omega\to+0}\mathrm{Im}\left[D_{\mathrm{m}}(\omega)\right]=(-\mathrm{sgn}\,\alpha)\infty \tag{25}$$

$$\lim_{\omega\to+0}\mathrm{Re}\left[V_{\mathrm{m}}(\omega)\right]=\alpha,\quad \lim_{\omega\to+0}\mathrm{Im}\left[V_{\mathrm{m}}(\omega)\right]=0\,. \tag{26}$$

Since the displacement and velocity due to seismic ground motion are causal functions, the real and imaginary parts of their Fourier spectra are in a Hilbert transform pair relationship. Therefore, it is sufficient to use only the real or imaginary part for the spectral fitting. According to Eqs. (25) and (26), both the step and pulse components have non-zero finite values in the limit of low frequency only in the real part of the displacement Fourier spectrum. Therefore, the spectral fitting is performed to determine t_{d}, t_{m}, α and β to minimize the evaluation function defined using the real part of the displacement Fourier spectrum:

$$P(t_{\mathrm{d}},t_{\mathrm{m}},\alpha,\beta)=\frac{\int_{\omega_1}^{\omega_2}\frac{1}{\omega}\left\{\mathrm{Re}\left[D(\omega)\right]-\mathrm{Re}\left[D_{\mathrm{m}}(\omega)\right]\right\}^2 d\omega}{\int_{\omega_1}^{\omega_2}\frac{1}{\omega}\left\{\mathrm{Re}\left[D(\omega)\right]\right\}^2 d\omega}, \tag{27}$$

where $D(\omega)$ is computed by dividing the acceleration Fourier spectrum by $-\omega^2$. Although the model displacement waveform constructed by the Gaussian-type basis function does not satisfy the causality strictly, the spectral fitting is performed in the same manner, assuming that its value in the range $t < 0$ is negligible. Integrals in the right-hand side of Eq. (27) are evaluated in the logarithmic scale of the angular frequency to weigh the low-frequency component relatively. The lower limit of the integral, ω_1, is determined to avoid contamination of the low-frequency noise, whereas the upper limit ω_2 is determined so that the spectrum does not deviate from the model spectrum due to vibration components of the seismic ground motion. Once the parameters t_{d} and t_{m} are assumed, α and β can be determined by the least square criterion. Therefore, the problem is reduced to the two-variable problem in the practice stage.

2.4 Estimation procedure of the displacement waveform

The procedure for estimating the displacement waveform of the ground motion in this study is summarized as follows.

(1) Adjust the baseline of the acceleration to let the mean of the pretrigger part go to zero.
(2) If the baseline of the acceleration seems to be changed during the ground motion, remove the offset of the baseline. The method proposed by Motoyama and Murono[8] is mainly used in this study, although a different method is used for some records.
(3) Compute the Fourier spectrum of the acceleration record and divide it by $-\omega^2$ to obtain the displacement Fourier spectrum.
(4) Search the optimum values of t_{d} and t_{m} computing the evaluation function.
(5) As shown in the following equation, construct a hybrid displacement spectrum $D_{\mathrm{h}}(\omega)$. In the hybrid spectrum, the original and model displacement Fourier spectra, $D(\omega)$ and $D_{\mathrm{m}}(\omega)$, respectively, are assigned on the high- and low-frequency side with a certain frequency f_{m} as the boundary. Finally, the hybrid displacement waveform is obtained as the inverse Fourier transform of $D_{\mathrm{h}}(\omega)$.

$$D_{\mathrm{h}}(\omega)=\left\{1-U\left(|\omega|-2\pi f_{\mathrm{m}}\right)\right\}D_{\mathrm{m}}(\omega)+U\left(|\omega|-2\pi f_{\mathrm{m}}\right)D(\omega) \tag{28}$$

Even in the vicinity of the source fault, a displacement that has the same amplitude to the positive and negative sides but does not cause the residual displacement may be observed. In such a case, it is sufficient to apply a low-cut filter after performing the above procedure (3) to remove the low-frequency noise because the value of the displacement Fourier spectrum is close to zero at low frequencies. Such

records also exist in the application examples shown in the next chapter.

3. APPLICATION EXAMPLES

3.1 Detection of step and pulse components and estimation of displacement waveform

As an example, the proposed method is applied to the strong ground motion record at the K-NET[16] Misumi site (KMM010, Uki City, Kumamoto Prefecture, Japan) during the mainshock of the Kumamoto earthquake (Mj7.3) that occurred on April 16, 2016. The site is located slightly away from the source fault, so the residual displacement is not very large. However, the east–west component of the displacement seems to consist of the step and pulse components, whereas the north–south component seems to be explained only by the pulse component. For this reason, it was selected as an example to examine the applicability of the proposed method.

First, the east–west component of the ground motion record at the K-NET Misumi site was examined. The first portion with the length of 100 s was considered from the start; then, the baseline was adjusted to let the pretrigger part with the length of 15 s be zero. Afterward, the baseline correction was applied using the Motoyama and Murono method[8] because a stepwise change in the acceleration baseline was observed. The Fourier spectrum was computed for the corrected acceleration record, and then the displacement Fourier spectrum was calculated by dividing it by $-\omega^2$. The parameters t_d, t_m, α and β were determined by spectral fitting using the Gaussian-, sine wave- and polynomial-type basis functions as described in Section 2.3, and then the hybrid displacement waveform was obtained.

Figure 3 shows the results of the spectral fitting. Panels (a), (b) and (c) show the distributions of the evaluation function values against t_d and t_m for the Gaussian-, sine wave- and polynomial-type basis functions, respectively. The cross symbol locates the optimum point that the evaluation function value is the minimum. Panel (d) shows the real parts of the displacement Fourier spectra of the observed ground motion and model displacement. From the displacement spectrum of the ground motion record shown in Fig. 3 (d), the lower limit of the fitting range was taken at 0.01 Hz in which the spectrum was insignificantly contaminated by the noise, whereas the upper limit was taken at 0.2 Hz in which the observed spectrum did not deviate from the model spectrum. The value of the evaluation function in Eq. (27) was calculated by converting the frequencies into angular frequencies as ω_1 and ω_2. The frequency connecting the observed and model spectra was set to 0.01 Hz according to the lower limit of the fitting range. Table 1 shows the optimum values of the estimated parameters for each basis function. From Figs. 3 (a)–(c) and Table 1, the values of the evaluation function were sensitive to t_d but insensitive to t_m, which was the same tendency as the spectral fitting to the trapezoidal function in the method proposed by Hirai[10]. According to Fig. 3 (d), the displacement Fourier spectrum of the ground motion record was strongly affected by the noise component in the frequency under 0.01 Hz. When a low-cut filter was used, the value of the spectrum in this range was considered zero; however, using the proposed method, it was replaced with the spectrum of the model displacement. Since the spectrum of the model displacement almost agreed with that of the ground motion record for each basis function, the step and pulse components contained in the ground motion record seemed to be well detected. In addition, there was almost no difference around the shape of the model spectra in the basis functions, which was because the difference in basis functions was reflected in the model displacement spectrum through the envelope shape $G'(\omega t_m)$ in Eq. (23); however, as shown in Fig. 2, the shape of that hardly depended on the types of basis functions. In this study, three types of basis functions were proposed: Gaussian, sine wave and polynomial types. However, from Fig. 3, almost the same displacement Fourier spectra were obtained regardless of which type of the basis function was employed. The polynomial-type basis function is assumed superior from the physical validity perspectives, namely, the causality and continuity of acceleration, but it is considered that any of them can be used in practice. Thus, hereinafter, only the polynomial-type basis function is used.

Figure 4 compares the model and hybrid displacements by the polynomial-type basis function with the ground motion record. The model displacement well represents the stepwise rise of the displacement

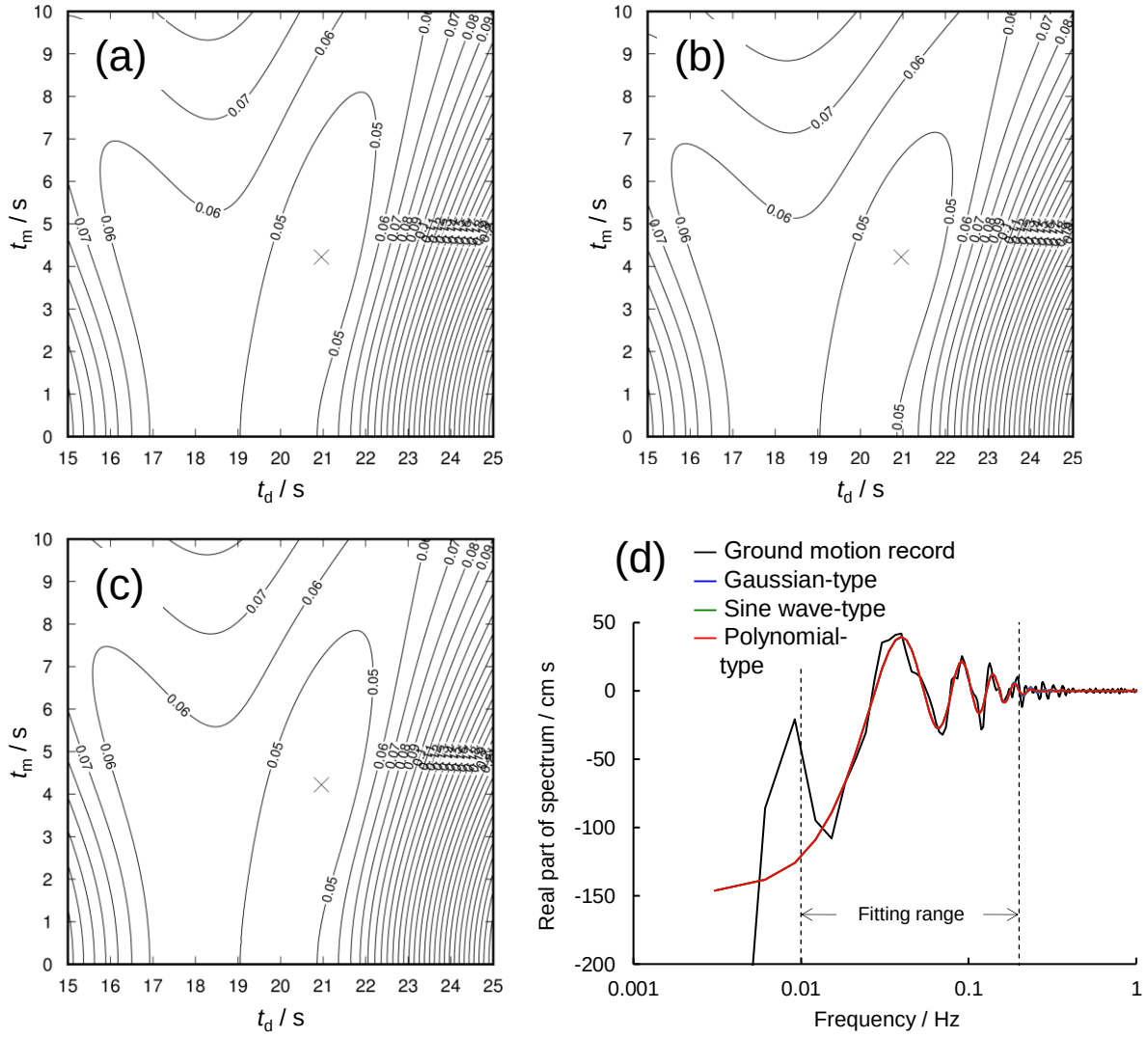

Fig. 3 Results of spectral fitting

Table 1 Parameters estimated by spectral fitting

Basis function	t_d / s	t_m / s	α / cm	β / cm
Gaussian-type	20.97	4.08	8.34	7.21
Sine wave-type	20.96	3.88	8.36	6.78
Polynomial-type	20.96	4.22	8.36	6.82

in the ground motion record and subsequent convergence to the residual displacement. From the results, when the displacement overshot and then converged to the final value, it was inappropriate to simulate the displacement using only the step component, whereas a reasonable estimation could be made by considering the pulse component. The hybrid displacement improved the convergence after the main tremor compared with the displacement from the observed ground motion.

Figure 5 shows the displacement waveforms estimated, applying the same procedure to the north–south component of the strong ground motion record at the K-NET Misumi site. Unlike the east–west component, almost only the pulse component was detected. The spectral fitting to the trapezoidal function proposed by Hirai[10] is based on the assumption that the step component is dominant throughout the displacement, whereas the proposed method is also applicable to the displacement in which the pulse

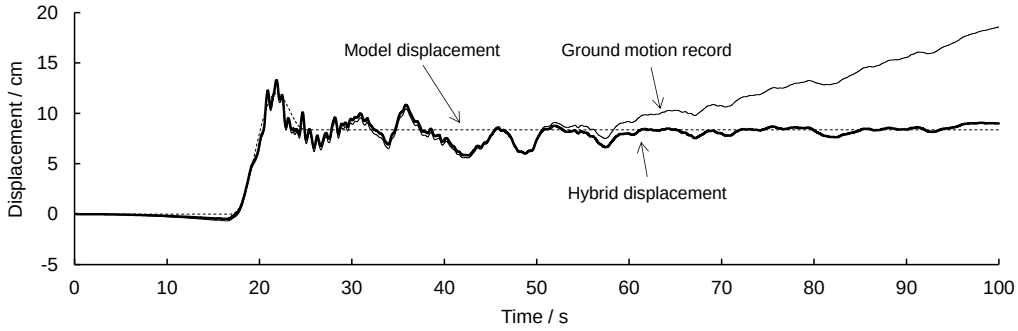

Fig. 4 East–west component of displacement at the K-NET Misumi site

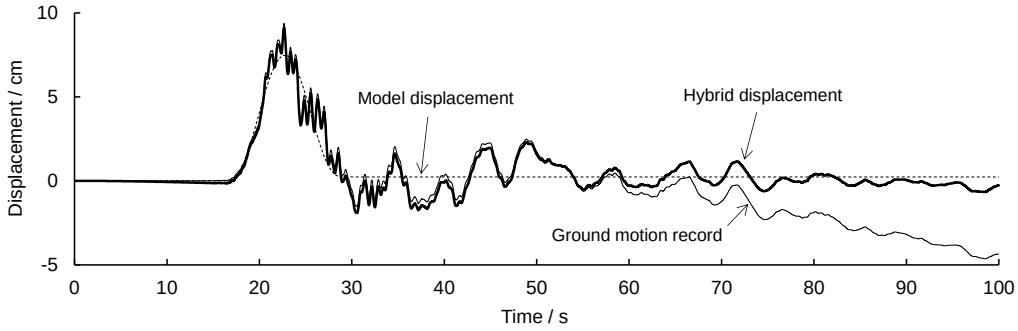

Fig. 5 North–south component of displacement at the K-NET Misumi site

component is dominant.

3.2 Comparison with the case of only the step component

In this study, the displacement of the ground motion was simulated by the sum of step and pulse components. Further, a comparison was made with the case where only the step component was assumed using the polynomial-type basis function. The east–west component of the strong ground motion record at the K-NET Misumi site during the mainshock of the 2016 Kumamoto earthquake was used for verification. The spectral fitting using only the step component and the construction of the hybrid displacement waveform were performed by fixing the magnitude of the pulse component β to zero in the formation shown in Section 2.3.

Figure 6 shows a comparison of the ground motion record, model and hybrid displacements. As in Section 3.1, the fitting range was 0.01–0.2 Hz, and the connecting frequency of spectra used to make the hybrid displacement was 0.01 Hz. The optimum values of the parameters obtained by the spectral fitting were $t_d = 18.68$ s, $t_m = 0.05$ s and $\alpha = 8.8$ cm. The hybrid displacement seemed to be a reasonable estimate, although the degree of agreement with the ground motion record before 50 s was slightly reduced compared with the result shown in Fig. 4. However, the rise time of the model displacement was very steep, reflecting that the estimated values of the parameters t_d and t_m were small. The reason for this feature is discussed below using the formulation and diagram of the displacement Fourier spectrum.

Figure 7 shows the real parts of the Fourier spectra for the displacement of the ground motion, the estimation results of each component when the step and pulse components were assumed, their sum and the model displacement when only the step component was assumed. As shown in Eq. (23), the real part of the displacement Fourier spectrum of the step component was $-G'(\omega t_m) \sin \omega t_d / \omega$, whereas that of the pulse component was $G'(\omega t_m) \cos \omega t_d$. As shown in Fig. 7, the phase delay in the frequency domain was caused by adding the latter to the former. When only the step component was assumed, the

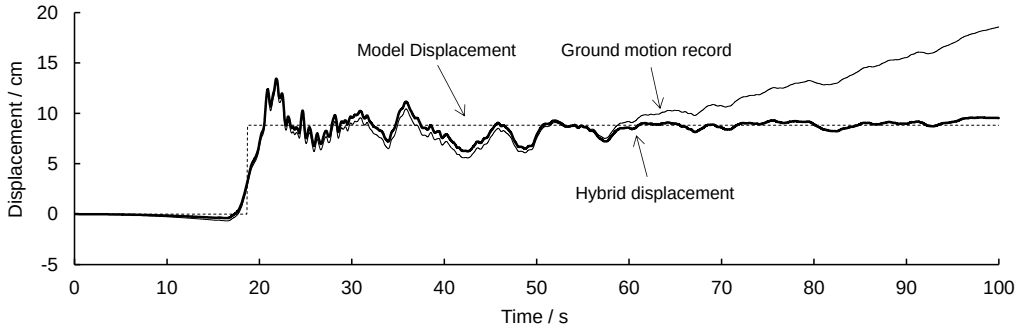

Fig. 6 East–west component of displacement at the K-NET Misumi site assuming only the step component

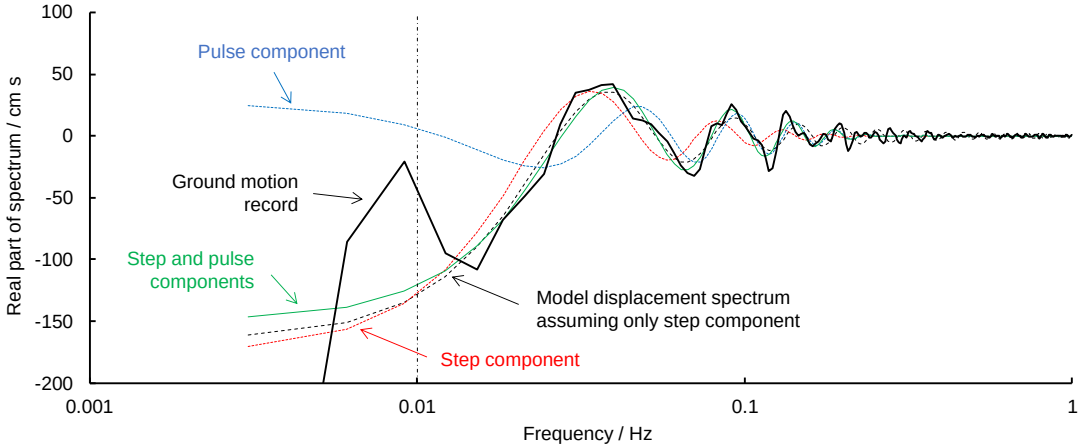

Fig. 7 Comparison of real parts of Fourier spectra

frequency of the carrier wave t_d decreased to fit the spectrum of the model displacement to that of the ground motion. However, because the amplitude of the model displacement became too small due to the effect of the factor $1/\omega$ in the spectrum of the step component, the parameter t_m was underestimated to let the envelope $G'(\omega t_m)$ attenuate slowly. Owing to these causes, when only the step component was assumed, both t_d and t_m were underestimated compared with when the spectral fitting including the pulse component was performed. For the ground motion record with a relatively large contribution of the step component, the displacement waveform could be estimated more reasonable by including the pulse component, although it is possible to do so assuming only the step component by the method proposed by Hirai[10].

3.3 Spatial distribution of the displacements of step and pulse components

The proposed method was applied to the strong ground motion records during the mainshock of the 2016 Kumamoto earthquake to investigate the spatial distribution of the displacements of the step and pulse components near the source fault. The records at ten sites of K-NET and KiK-net located within the epicentral distance of 30 km were used: Tamana (KMM003), Ohzu (KMM005), Kumamoto (KMM006), Uto (KMM008), Yabe (KMM009), Misumi (KMM010), Tomochi (KMM11), Kikuchi (KMMH03), Toyono (KMMH14) and Mashiki (KMMH16).

The stepwise changes in the acceleration baseline were corrected at first for the east–west and north–south components of the acceleration record at each site using the Motoyama and Murono method[8]. However, only the north–south component of KMM011 had a negative time of the baseline change, so appropriate results could not be obtained. Therefore, the baseline correction was applied to

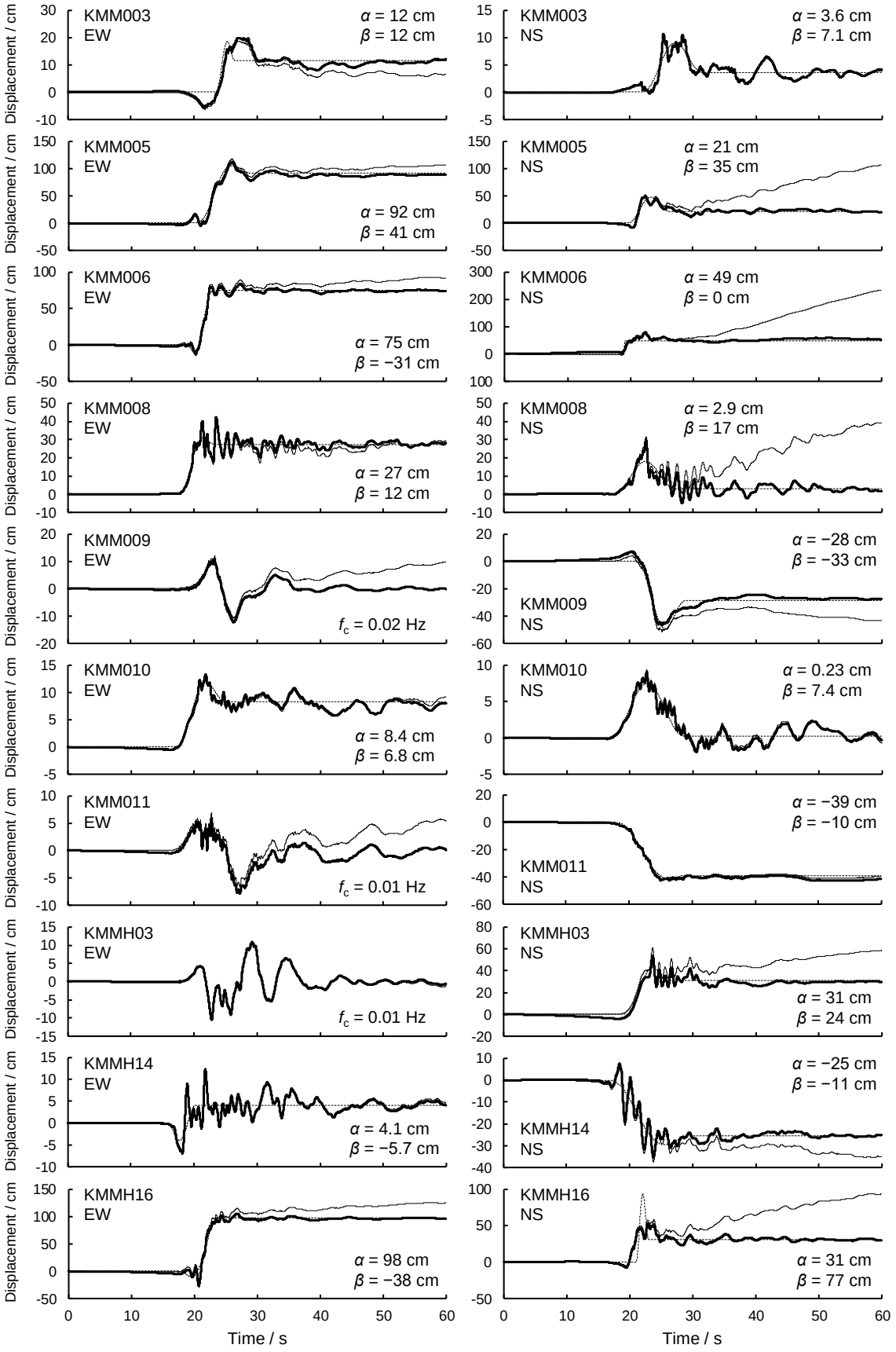

Fig. 8 Displacements at each site near the source fault of the mainshock of the Kumamoto earthquake

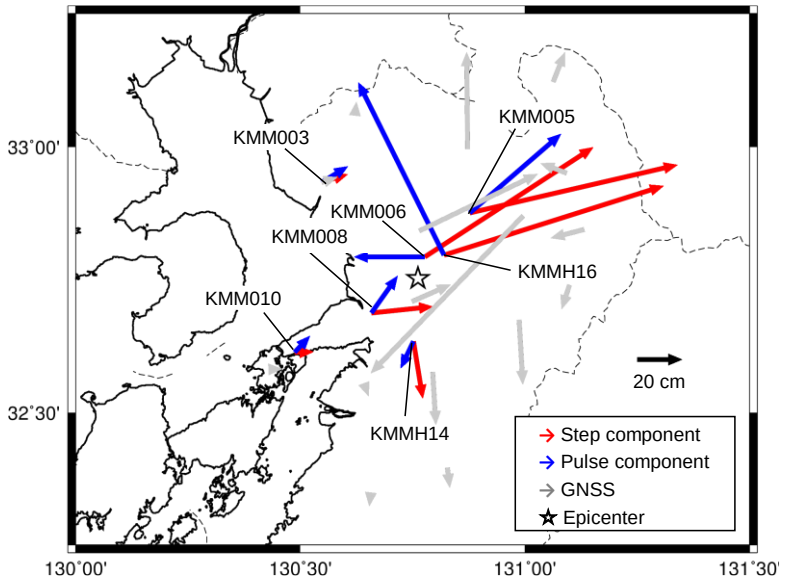

Fig. 9 Spatial distribution of displacement by the mainshock of the Kumamoto earthquake

the record by subtracting the slope determined by linear approximation of the range 30–60 s of the velocity waveform, which was considered to be after the main tremor. From the records, the correction method of the acceleration baseline might not give appropriate results for some records. Although the cause and solution for the problem are interesting subjects, they will not be discussed in detail in this article.

Figure 8 shows the results of the application of the proposed method to the strong ground motion records at each site. Thin solid, broken and thick solid lines represent the displacement of the ground motion record, model and hybrid displacements, respectively. The estimated magnitudes of the step component α and pulse component β are shown for each record. The fitting range was 0.01–0.2 Hz, and the connection frequency of the spectra to generate the hybrid displacement was 0.01 Hz. However, for the east–west component of KMM008 and the north–south component of KMM005, KMM006, KMM008 and KMMH16, the low-frequency noise was rather large, so the fitting range was 0.03–0.2 Hz, and the connection frequency was 0.03 Hz. For the east–west components of KMM009, KMM011 and KMMH03, because the step and pulse components were small and the displacement waveform seemed to be a both-sided swaying, the proposed method was not applied; only a low-cut filter was applied. In this case, the value of the cut-off frequency f_c is shown in the figure. From Fig. 8, the step and pulse components were detected, and the displacement waveform was synthesized appropriately. Even if the displacement of the ground motion record increases linearly after the main tremor, as in the north–south component of KMM005, the hybrid displacement converges to an almost constant value.

Figure 9 shows the spatial distribution of the horizontal displacement separating to the step and pulse components at each site for which the step and pulse components could be estimated for both the east–west and north–south components. The figure also shows the displacements detected by the GNSS continuous observation network, GEONET[17], for one day across the mainshock of the 2016 Kumamoto earthquake. Although they included not only the effect of the mainshock but also the aftershocks, their contribution to the residual displacement was negligible because the magnitude of the mainshock was 7.3 and that of the largest aftershock was 5.9. Therefore, it could be considered that the distribution of the step displacement component and displacement by GNSS also showed the spatial distribution of crustal deformation due to the mainshock. Although it was difficult to compare directly becasue the spatial distribution of the strong ground motion observation sites and the GNSS sites were not the same, the direction and amount of displacement showed a similar tendency for close sites. Thus, the step displacement component, namely, the residual displacement, obtained by the proposed method was almost consistent with the observation results by GNSS. The amount of displacement of the pulse component was almost the same as that of the step component at most sites, whereas the direction of the

displacement might be close to that of the step component or it might be significantly different. Such a distribution is considered to reflect the rupture process of the source fault. However, because the actual direction and amount of the fault slip is nonuniform, it is difficult to understand the source process with only a simplified model such as the step and pulse components. To understand the actual source process, detailed techniques, such as the waveform inversion analysis (e.g., Yoshida et al.[18]), are necessary.

4. CONCLUSIONS AND FUTURE ISSUES

In this study, a method for detecting the step and pulse displacement components contained in seismic ground motion near the source fault using spectral fitting was proposed. As basis functions to simulate each component, a polynomial-type basis function that satisfies the causality and continuity of acceleration was proposed in addition to the Gaussian- and sine wave-type functions that have been used in other studies. Further, the displacement waveform was estimated by connecting the spectra of the ground motion record and model displacements instead of suppressing the low-frequency noise via a low-cut filter. Applying the proposed method to the strong ground motion record at the K-NET Misumi site during the mainshock of the 2016 Kumamoto earthquake, the step and pulse components contained in the ground motion were detected, and an appropriate displacement waveform was estimated. Compared with a method in which only the step component was assumed, a more reasonable displacement was estimated by assuming the step and pulse components. In addition, almost the same results were obtained using any of the three basis functions. Besides, applying the proposed method to several strong ground motion records obtained at near-fault sites during the mainshock of the Kumamoto earthquake, the spatial distribution of the displacement agreed with that of GNSS.

Although the parameters are determined by spectral fitting in the proposed method, the fitting range must be set depending on the ground motion record. Since the decision is made by sight, it is unsuitable for automatic processing and may be affected by artificial biases. The determination technique of the fitting range may be improved in the future.

ACKNOWLEDGMENT

Ms. Misa Moriwaki, a former graduate student of Nagoya University, made the great deal of effort to this study. The public data of the strong ground motion-observation network K-NET and KiK-net provided by the National Research Institute for Earth Science and Disaster Resilience were used as the seismic ground motion record to be examined. The public data of the GNSS provided by the Geospatial Information Authority of Japan was also used. Some diagrams in this paper were made by Generic Mapping Tools[19]. Three anonymous reviewers provided beneficial suggestions. The author would like to express a gratitude to each of them. This article was made as an English version of the original article written in Japanese[20]. The author would like to thank Enago (www.enago.jp) for the English language review.

REFERENCES

1) Iwata, T.: The Report of Three Months from the Kumamoto Earthquake, *Public Symposium of Science Council of Japan*, 20 pp., 2016 (in Japanese).
2) Graizer, V. M.: Effect of Tilt on Strong Motion Data Processing, *Soil Dynamics and Earthquake Engineering*, Vol. 25, No. 3, pp. 197–204, 2005.
3) Boore, D. M.: Effect of Baseline Corrections on Displacements and Response Spectra for Several Recordings of the 1999 Chi-Chi, Taiwan, Earthquake, *Bulletin of the Seismological Society of America*, Vol. 91, No. 5, pp. 1199–1211, 2001.
4) Ohta, Y. and Aydan, O.: An Integration Technique for Ground Displacement from Acceleration Records and Its Application to Actual Earthquake Records, *Journal of The School of Marine Science*

and Technology, Tokai University, Vol. 5, No. 2, pp. 1–12, 2007 (in Japanese).
5) Hirai, T. and Fukuwa, N.: Estimation of Crustal Deformation Distribution due to the 2011 off the Pacific Coast of Tohoku Earthquake Based on Strong Motion Records, *Journal of Structural and Construction Engineering (Transactions of AIJ)*, Vol. 77, No. 673, pp. 341–350, 2012 (in Japanese).
6) Iwan, W., Moser, M. and Peng, C.: Some Observations on Strong-Motion Earthquake Measurement Using a Digital Accelerograph, *Bulletin of the Seismological Society of America*, Vol. 75, No. 5, pp. 1225–1246, 1985.
7) Javelaud, E. H., Ohmachi, T. and Inoue, S.: A Quantitative Approach for Estimating Coseismic Displacements in the Near Field from Strong-Motion Accelerographs, *Bulletin of the Seismological Society of America*, Vol. 101, No. 3, pp. 1182–1198, 2011.
8) Motoyama, H. and Murono, Y.: Calculation Technique to Acquire Displacement from Seismic Acceleration Records, *Journal of the Japan Society of Civil Engineers*, A1, Vol. 68, No. 4, pp. I_202–I_208, 2012 (in Japanese).
9) Hayashi, Y., Katukura, H, Watanabe, T., Kataoka, S., Yokota, H. and Tanaka, T.: Reliability of Integrated Displacements from Accelerograms by Digital Accelerographs, *Journal of Structural and Construction Engineering (Transactions of AIJ)*, No. 419, pp. 57–66, 1991 (in Japanese).
10) Hirai, T.: Estimation of Ground Displacement from Seismic Acceleration Record by Spectral Fitting to Trapezoidal Function, *Journal of Structural and Construction Engineering (Transactions of AIJ)*, Vol. 83, No. 751, pp. 1229–1238, 2018 (in Japanese).
11) Hirai, T.: Detection of the Step and Pulse Components Contained in the Near-Fault Ground Motion Record and Estimation Method of Displacement Waveform, *Proceedings of 2019 Annual Meeting of Japan Association for Earthquake Engineering*, P2–4, 2019 (in Japanese).
12) Kostadinov, M. V. and Yamazaki, F.: Influence of Static Displacement on Peak Ground Velocity at Sites that Experienced Forward-Rupture Directivity, *Proceedings of Workshop on Seismic Fault-Induced Failures*, pp. 115–120, 2001.
13) Okazawa, R., Sugino, M. and Hayashi, Y.: Modeling of Super High-Rise Buildings and Response Properties Against Ricker Wavelet—Damage Prediction for Super High-Rise Buildings in Osaka Against Pulse-Like Ground Motions Part 1—, *Journal of Structural and Construction Engineering (Transactions of AIJ)*, Vol. 83, No. 745, pp. 421–430, 2018 (in Japanese).
14) Moriwaki, M.: Development of the Method Evaluating the Ground Displacement Using the Seismic Acceleration Record and Analysis of the Near-Fault Ground Motion, *Dissertation of Master of Engineering*, Graduate School of Environmental Studies, Nagoya University, 88 pp., 2019 (in Japanese).
15) Yasumoto, H., Okazawa, R., Takiyama, N., Onishi, Y. and Hayashi, Y.: Maximum Response Evaluation of Based-Isolated Buildings Against Pulse-Like Ground Motions in Case of Collision to Retaining Wall, *Journal of Structural and Construction Engineering (Transactions of AIJ)*, Vol. 79, No. 697, pp. 385–392, 2014 (in Japanese).
16) National Research Institute for Earth Science and Disaster Resilience: Strong-Motion Seismograph Networks (K-NET, KiK-net). https://www.kyoshin.bosai.go.jp/ (last accessed on November 21, 2019)
17) Geospatial Information Authority of Japan: Service of GSI's GNSS Stations Data. https://www.gsi.go.jp/ENGLISH/geonet_english.html (last accessed on November 21, 2019)
18) Yoshida, K., Miyakoshi, K., Somei, K. and Irikura, K.: Source Process of the 2016 Kumamoto Earthquake (Mj7.3) Inferred from Kinematic Inversion of Strong-Motion Records, *Earth, Planets and Space*, Vol. 69, 64, 2017.
19) Wessel, P., Smith, W. H. F., Scharroo, R., Luis, J. F. and Wobbe, F.: Generic Mapping Tools: Improved Version Released, *EOS Transactions of American Geophysical Union*, Vol. 94, No. 45, pp. 409–410, 2013.
20) Hirai, T.: Detection of Step and Pulse Components and Estimation of Displacement Waveform Based on Near-Fault Seismic Ground Motion Record, *Journal of Japan Association for Earthquake Engineering*, Vol. 20, No. 6, pp. 6_1–6_14, 2020.

(Original Japanese Paper Published: August, 2020)
(English Version Submitted: November 29, 2021)
(English Version Accepted: December 28, 2021)